THE JOURNAL OF PHYSICAL CHEMISTRY A

Article

Cite This: J. Phys. Chem. A 2018, 122, 5361−5369

pubs.acs.org/JPCA

Energy-Transfer Kinetics for Xe (6p[1/2]$_0$) Atoms in Kr, Ar, Ne, and He

Shan He,[†,‡] Dong Liu,[†] Xueyang Li,[†,‡] Junzhi Chu,[†,‡] Jingwei Guo,*[,†] Jinbo Liu,[†] Shu Hu,[†] Fengting Sang,[†] and Yuqi Jin[†]

[†]Key Laboratory of Chemical Lasers, Dalian Institute of Chemical Physics, Chinese Academy of Sciences, Dalian, 116023, P. R. China

[‡]University of Chinese Academy of Sciences, Beijing, 100049, P. R. China

ABSTRACT: The kinetic processes for the Xe (6p[1/2]$_0$) atoms in Kr, Ar, Ne, and He buffer gases were studied. We found that Kr, Ar, and Ne atoms can be used to switch the amplified spontaneous emission (ASE) channel from 3408 nm (6p[1/2]$_0$−6s′[1/2]$_1$) to 3680 nm (5d[1/2]$_1$−6p[1/2]$_1$), while Xe and He atoms do not show such a phenomenon. This ASE channel switch is mainly ascribed to the fast transfer of 6p[1/2]$_0$ → 5d[1/2]$_1$. On the basis of the rate equations for two-state coupling (energy-transfer processes between the two states are very rapid), the reason why the ASE channel switch effect normally coincides with a double exponential decay of the spontaneous emission at 828 nm (6p[1/2]$_0$−6s[3/2]$_1$) is explained. The actual situations in Xe, Ar, Ne, and He follow this rule. However, the strictly single exponential decay of the spontaneous emission at 828 nm and strong ASE channel switch effect simultaneously emerge in Kr. This indicates that the transfer of 6p[1/2]$_0$ → 5d[1/2]$_1$ in Kr does not occur via two-state coupling, but via two steps of near-resonance collision through the 5s[3/2]$_2$ (Kr) state as the intermediate state (6p[1/2]$_0$ → 5s[3/2]$_2$ (Kr) → 5d[1/2]$_1$). In addition, we found Xe (6p[1/2]$_0$) atoms strongly tend to reach the 6p[3/2]$_2$, 6p[3/2]$_1$, and 6p[5/2]$_2$ states through the 5s[3/2]$_2$ (Kr) state as the intermediate state in Kr. The 5s[3/2]$_2$ (Kr) state plays a very important role in the energy-transfer kinetics for the Xe (6p[1/2]$_0$) atoms. Kr is probably an excellent buffer gas for laser systems based on Xe.

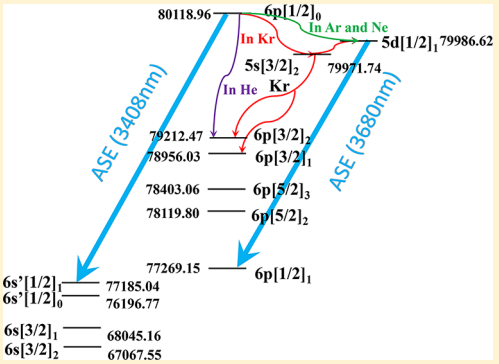

I. INTRODUCTION

Recently, a diode-pumped metastable rare gas laser (DPRGL) was proposed as a potential high-energy laser system.[1] This new system has many advantages such as mild working conditions, an inert chemical property, and abundant states. Therefore, many groups have investigated this system.[2−8] High Ar (5s[3/2]$_2$) concentrations and optical efficiency (55%) have been obtained.[4,5] Heaven and co-workers have demonstrated a CW diode-pumped Ar* laser providing 4 W.[6] However, abundant states can result in complex kinetics between the excited states. It is of great importance to study the kinetic processes between the excited states before selecting a reasonable laser system.

It is easier to produce metastable Xe atoms in comparison with Ne, Ar, and Kr atoms, which is a positive aspect for realizing a DPRGL. However, the energy differences among the low-lying excited states for Xe are smaller than those for lighter rare gases. As a result, the kinetic processes among the excited states of Xe are more complex. Many researchers have studied the kinetics between the excited states of Xe.[9−18] Only when the kinetic process is definited, the lifetimes and decay rate constants for the excited states of Xe can be accurately deduced. To avoid the risk of triggering unexpected processes, the excitation laser powers used in these studies are relatively low.[15,16] However, the laser systems always prefer a high power of pump sources. Therefore, it is of great significance to figure out the kinetics between the excited states of Xe under high excitation laser power conditions.

In our previous work, we have studied the kinetic processes for Xe (6p[1/2]$_0$) atoms under high excitation laser power conditions and found that the intense excitation laser can trigger amplified spontaneous emission (ASE) at 3408 nm (6p[1/2]$_0$−6s′[1/2]$_1$).[19] This ASE can lead to a substantial number of 6s′[1/2]$_1$ atoms being produced. By virtue of the small energy difference between the 6p[1/2]$_1$ and 6s′[1/2]$_1$ states (84 cm^{-1}) and high collision rate constant for transfer from the 6s′[1/2]$_1$ to the 6p[1/2]$_1$ state, the 6s′[1/2]$_1$ atoms can readily arrive at the 6p[1/2]$_1$ state. Therefore, the intense fluorescence was observed at a wavelength of 980 nm (6p[1/2]$_1$−6s[3/2]$_2$). All these processes can be described concisely as eqs 1−4:

$$\mathrm{Xe}(s_0) \xrightarrow{\text{laser}} \mathrm{Xe}(6p[1/2]_0) \quad (1)$$

$$\mathrm{Xe}(6p[1/2]_0) \xrightarrow{\text{ASE(3408 nm)}} \mathrm{Xe}(6s'[1/2]_1) \quad (2)$$

$$\mathrm{Xe}(6s'[1/2]_1) + \mathrm{Xe}(s_0) \xrightarrow{\text{collision}} \mathrm{Xe}(6p[1/2]_1) + \mathrm{Xe}(s_0) \quad (3)$$

$$\mathrm{Xe}(6p[1/2]_1) \xrightarrow{\text{fluorescence(980 nm)}} \mathrm{Xe}(6s[3/2]_2) \quad (4)$$

Received: April 5, 2018
Revised: May 28, 2018
Published: May 29, 2018

DOI: 10.1021/acs.jpca.8b03238
J. Phys. Chem. A 2018, 122, 5361−5369

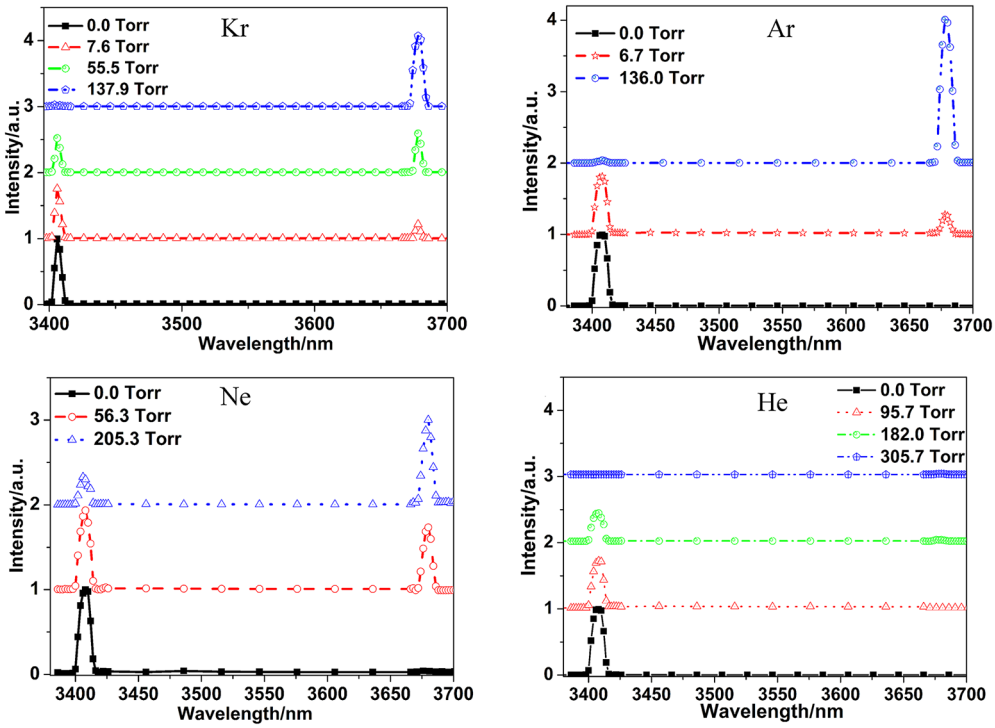

Figure 1. ASE spectra for Xe ($6p[1/2]_0$) in the forward direction along the laser axis for varying Kr, Ar, Ne, and He pressures. The laser prepared state is the $6p[1/2]_0$ state. The Xe pressure was kept constant at 8.0 Torr. The pressures listed in these plots are the pressures of the buffer gases. The energy of the excitation laser is 3.86 mJ. For clear comparison, the intensity measured under different conditions is moved upward 1 au stepwise.

Buffer gases play a crucial role in the transitions from the excited states to the upper states of a laser in three-level systems. In optically pumped alkali vapor lasers (DPAL), methane or ethane are often added into the system to accelerate this transfer.[20] In this work, the kinetic processes for Xe ($6p[1/2]_0$) atoms in buffer gases including Kr, Ar, Ne, and He are studied. An ASE channel switch effect appears when Kr, Ar or Ne is used as the buffer gas. These three gases can switch the ASE channel from 3408 nm ($6p[1/2]_0$–$6s'[1/2]_1$) to 3680 nm ($5d[1/2]_1$–$6p[1/2]_1$). This is due to the strong tendency for the transfer of $6p[1/2]_0 \rightarrow 5d[1/2]_1$. The primary mechanism for accelerating the transfer of $6p[1/2]_0 \rightarrow 5d[1/2]_1$ in Ar and Ne is two-state coupling. On the basis of a calculation model, the transfer constants for Ar and Ne were deduced. The value for $k^{Ar}_{6p[1/2]_0,5d[1/2]_1}$ is higher than that for $k^{Ne}_{6p[1/2]_0,5d[1/2]_1}$. Accordingly, the ASE channel switch effect for Ar is stronger than that for Ne. However, the primary mechanism in Kr is probably accomplished by two steps of near-resonance collision through the $5s[3/2]_2$ (Kr) state as the intermediate state ($6p[1/2]_0 \rightarrow 5s[3/2]_2$ (Kr) $\rightarrow 5d[1/2]_1$). The Kr atoms can accelerate not only the transfer of $6p[1/2]_0 \rightarrow 5d[1/2]_1$ but also the transfers of $6p[1/2]_0 \rightarrow 6p[3/2]_2$, $6p[3/2]_1$, $6p[5/2]_2$. He atoms cannot accelerate the transfer of $6p[1/2]_0 \rightarrow 5d[1/2]_1$. Accordingly, no new ASE peak emerges when a He buffer gas is used. The primary kinetic process in He is relaxation, and the transfer of $6p[1/2]_0 \rightarrow 6p[3/2]_2$ takes a great probability of the total relaxation in He. Throughout this paper, if not specified, all electronic states refer to the states of Xe.

II. EXPERIMENTAL METHODS

The experimental apparatus was described in our previous work.[19] Thus, only a brief description is given here. A Nd:YAG laser (Beamtech SGR-10) was used to pump a dye laser (Sirah CBST-LG-18-EG). A tunable laser beam in the range from 480 to 540 nm was obtained. Then, a BBO crystal was utilized to frequency-double this tunable laser beam to generate a tunable ultraviolet laser beam. A series of Pellin–Broca prisms were used to separate the ultraviolet beam from the fundamental beam. The Xe ($6p[1/2]_0$) atoms were prepared by two-photon excitation at a wavelength of ~249.5 nm. The full width at half-maximum for the ultraviolet beam is ~7 ns. A power meter (Gentec QE 12LP-S-MB-D0) was used to monitor the power of the laser.

A stainless-steel cell with four windows was used to contain the gases. One window of the cell was made of sapphire to ensure that the MIR (mid-infrared) ASE passes through the window. The other three windows were made of fused quartz. Ultrahigh purity Xe (99.999%), Kr (99.999%), Ar (99.999%), Ne (99.999%), and He (99.999%) were used. A manometer (UNIK 5000) was used to measure the pressures of the gases.

A series of lenses were placed along the axis perpendicular to the excitation laser to collect the fluorescence. Then, the fluorescence was dispersed by a monochromator (Princeton Instrument SpectraPro 2500i) equipped with a 1200 g/mm grating. The specific spontaneous emission line was detected by an avalanche photodiode (APD 430 A) and recorded by an oscilloscope (LeCroy waverunner 620zi). All the time-resolved signals were averaged over 200 shots.

An uncoated Si plate was placed along the laser axis and behind the gas cell to absorb the excitation laser and transmit the MIR ASE. The MIR ASE was dispersed by a monochromator (HORIBA micro HR MHRA-2A-MS) equipped with a 300 g/mm infrared grating. Then, the MIR ASE was measured by a photodiode (InSb). The distance between the sapphire window of the cell and the monochromator was set to 20 cm to avoid interference from the divergence of the ASE.

DOI: 10.1021/acs.jpca.8b03238
J. Phys. Chem. A 2018, 122, 5361–5369

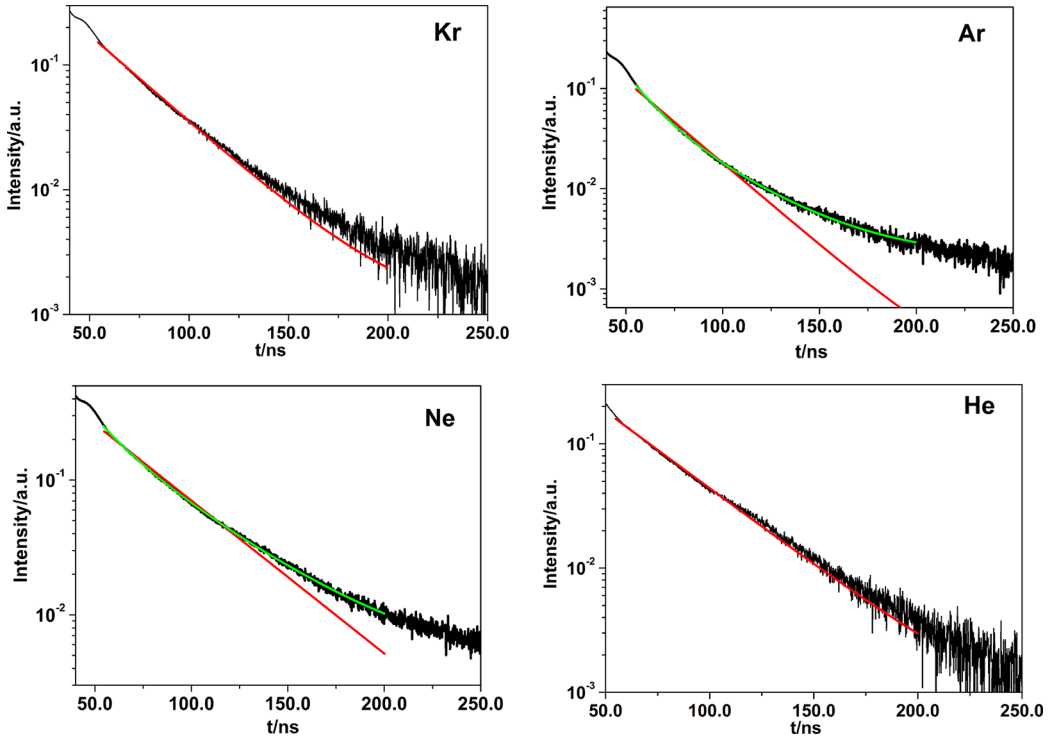

Figure 2. Time-resolved fluorescence curves measured at 828 nm for different buffer gases. The plots marked with Kr, Ar, Ne, and He were acquired under the conditions of (p_{Xe} = 4.0 Torr) + (p_{Kr} = 3.0 Torr), (p_{Xe} = 4.0 Torr) + (p_{Ar} = 4.9 Torr), (p_{Xe} = 4.0 Torr) + (p_{Ne} = 9.0 Torr), and (p_{Xe} = 4.0 Torr) + (p_{He} = 14.0 Torr), respectively. The black lines show the experimental data. The red and blue lines are fitting lines for a single and double exponential decay function, respectively. The energy of the excitation laser is 2.80 mJ.

III. RESULTS AND DISCUSSION

The MIR spectra for the Xe ($6p[1/2]_0$) atoms in different pressures of Kr, Ar, Ne, and He are shown in Figure 1. An interesting phenomenon emerges. The intensity of the ASE at 3408 nm ($6p[1/2]_0$–$6s'[1/2]_1$) gradually decreases, and a brand new ASE at 3680 nm appears and gradually increases when Kr, Ar, and Ne are added into the cell. The wavelength of this new ASE exactly corresponds to the transition of $5d[1/2]_1$–$6p[1/2]_1$. The energy difference between the $6p[1/2]_0$ state and the $5d[1/2]_1$ state is only ~132 cm^{-1}. Kr, Ar, and Ne may accelerate the transfer of $6p[1/2]_0 \rightarrow 5d[1/2]_1$. However, no new ASE occurs when a He buffer gas is used. The intensity of the ASE at 3408 nm ($6p[1/2]_0$–$6s'[1/2]_1$) gradually decreases with increasing He pressure. He atoms may not have the ability to selectively accelerate the transfer of $6p[1/2]_0 \rightarrow 5d[1/2]_1$. In addition, more He atoms result in a higher probability of relaxation. This reduces the probability for ASE at 3408 nm ($6p[1/2]_0$–$6s'[1/2]_1$). This is the so-called quenching effect.

Another interesting result reported in previous studies is that the high rate constant for the transfer of $6p[1/2]_0 \rightarrow 5d[1/2]_1$ always accompanies a double exponential decay of the $6p[1/2]_0$ state.[10,12,15] If the buffer gas atoms do not result in a high rate constant for the transfer of $6p[1/2]_0 \rightarrow 5d[1/2]_1$, the decay curves for 828 nm ($6p[1/2]_0$–$6s[3/2]_1$) strictly follow a single exponential decay. Setser and co-workers have found that the decay curves for 828 nm ($6p[1/2]_0$–$6s[3/2]_1$) in buffer gases of Ar and Ne fit a double exponential decay, while those in Xe, Kr, and He fit a single exponential decay.[9,10,12] To identify this phenomenon, the decay curves for 828 nm ($6p[1/2]_0$–$6s[3/2]_1$) were measured and fitted in these gases, as shown in Figure 2. Clearly, the decay curves for 828 nm ($6p[1/2]_0$–$6s[3/2]_1$) in Ar and Ne buffer gases both deviate from a single exponential decay function, while those in He and Kr fit a single exponential decay function. Our previous work has proven that the decay curves for 828 nm in Xe also fit a single exponential decay function.[19] It can be deduced that the rate constant for the transfer of $6p[1/2]_0 \rightarrow 5d[1/2]_1$ in Ar and Ne is relatively high, while that in Xe, He, and Kr should be low. On the basis of this phenomenon, one can predict that the Ar and Ne atoms should show an ASE channel switch effect and that Xe, He, and Kr atoms should not show this effect. The actual situations in Xe, Ar, Ne, and He all fit such a prediction. However, Kr is an exception. To determine the relationship between the high transfer rate constant for $6p[1/2]_0 \rightarrow 5d[1/2]_1$ and decay function for 828 nm ($6p[1/2]_0$–$6s[3/2]_1$), the following derivations are made. The rate equations for the energy-transfer processes between the $6p[1/2]_0$ state and the $5d[1/2]_1$ state can be written as eqs 5 and 6.

$$\frac{d[6p[1/2]_0]}{dt} = -(k^{Rg}_{6p[1/2]_0,T}[Rg] + k^{Xe}_{6p[1/2]_0,T}[Xe] + k_{6p[1/2]_0,r})[6p[1/2]_0] + (k^{Rg}_{5d[1/2]_1,6p[1/2]_0}[Rg] + k^{Xe}_{5d[1/2]_1,6p[1/2]_0}[Xe])[5d[1/2]_1] \quad (5)$$

$$\frac{d[5d[1/2]_1]}{dt} = -(k^{Rg}_{5d[1/2]_1,T}[Rg] + k^{Xe}_{5d[1/2]_1,T}[Xe] + k_{5d[1/2]_1,r})[5d[1/2]_1] + (k^{Rg}_{6p[1/2]_0,5d[1/2]_1}[Rg] + k^{Xe}_{6p[1/2]_0,5d[1/2]_1}[Xe])[6p[1/2]_0] \quad (6)$$

where $k^{Rg}_{i,T}$ is the total decay rate constant of the i state due to collision with rare gas atoms, $k^{Xe}_{i,T}$ is the total decay rate constant

DOI: 10.1021/acs.jpca.8b03238
J. Phys. Chem. A 2018, 122, 5361−5369

of the i state due to collision with Xe atoms, $k_{i,r}$ is the radiative decay rate of the i state, $k_{i,j}^{Rg}$ is the rate constant of the transfer of $i \rightarrow j$ due to collision with Rg atoms, and $k_{i,j}^{Xe}$ is the rate constant of the transfer of $i \rightarrow j$ due to collision with Xe atoms. To concisely express the equations, the following definitions are made:

$$A_{11} = k^{Rg}_{6p[1/2]_0,T}[Rg] + k^{Xe}_{6p[1/2]_0,T}[Xe] + k_{6p[1/2]_0,r},$$
$$A_{21} = k^{Rg}_{5d[1/2]_1,6p[1/2]_0}[Rg] + k^{Xe}_{5d[1/2]_1,6p[1/2]_0}[Xe],$$

$$A_{22} = k^{Rg}_{5d[1/2]_1,T}[Rg] + k^{Xe}_{5d[1/2]_1,T}[Xe] + k_{5d[1/2]_1,r},$$
$$A_{12} = k^{Rg}_{6p[1/2]_0,5d[1/2]_1}[Rg] + k^{Xe}_{6p[1/2]_0,5d[1/2]_1}[Xe],$$

$$N_1 = [6p[1/2]_0], \quad N_2 = [5d[1/2]_1]$$

Then, eqs 5 and 6 can be rewritten as eqs 7 and 8:

$$-A_{11}N_1 + A_{21}N_2 = \frac{dN_1}{dt} \tag{7}$$

$$A_{12}N_1 - A_{22}N_2 = \frac{dN_2}{dt} \tag{8}$$

The solutions for eqs 7 and 8 have the following general form:

$$N_i = a_{i1}e^{-\lambda_+ t} + a_{i2}e^{-\lambda_- t} \tag{9}$$

$\lambda_{+,-}$ are the two eigenvalues for eq 10:

$$\begin{vmatrix} \lambda - A_{11} & A_{21} \\ A_{12} & \lambda - A_{22} \end{vmatrix} = 0 \tag{10}$$

$k_{5d[1/2]_1,6p[1/2]_0}$ (denoted as k_{21}) and $k_{6p[1/2]_0,5d[1/2]_1}$ (denoted as k_{12}) obey the following relationship:[12,15,21]

$$\frac{N_1}{N_2} = \frac{g_1 e^{-\varepsilon_1/kT}}{g_2 e^{-\varepsilon_2/kT}} = \frac{k_{21}}{k_{12}} \tag{11}$$

Then, the relationship between k_{21} and k_{12} can be expressed as $k_{21} = k_{12}/5.66$. Under the condition of pure Xe, all the [Rg] = 0. The value of $k_{1,2}^{Xe}$ is relatively small (smaller than 0.58×10^{-11} cm^3 s^{-1}).[9,19] Then, the value of $k_{2,1}^{Xe}$ is even smaller. Thus, the A_{21} can be omitted in eq 7. Then, eq 7 can be rewritten as eq 12:

$$-A_{11}N_1 = \frac{dN_1}{dt} \tag{12}$$

It is easy to deduce $N_1 = a_{11}e^{-A_{11}t}$. Thus, the fluorescence at 828 nm shows a single exponential decay in pure Xe. In addition, the $k_{2,1}^{Kr}$ and $k_{2,1}^{He}$ values should be low enough to be omitted. Therefore, the decay curves for 828 nm ($6p[1/2]_0$–$6s[3/2]_1$) in He and Kr fit the single exponential function. Then, the total decay rate constants for He and Kr can be deduced by a Stern–Volmer plot. These plots are shown in Figure 3. The total decay rate constants for Kr and He are listed in Table 1.

If the value for k_{12} is high, the value for k_{21} is also high. Then, A_{21} in eq 7 cannot be omitted. Therefore, the decay curve at 828 nm fits a double exponential function. However, under the condition that the p_{Xe} is relatively high and p_{Rg} (Rg = Ar or Ne) is very low, the decay curve at 828 nm may also fit a single exponential function. Although the $k_{1,2}^{Rg}$ (Rg = Ar or Ne) is relatively high, the A_{12} is not very high for low pressures of Ar or Ne. Thus, the density of N_2 is not very high. Equally, $k_{2,1}^{Rg} \times$ [Rg] (Rg = Ar or Ne) is not very high for low pressures of Ar or Ne. This leads to a relatively low A_{12}. Moreover, the high value of p_{Xe} results in a high value for $A_{11}N_1$. Therefore, the parameter $A_{21}N_2$ in eq 7 can be omitted. To obtain the total decay rate constants for Ar and Ne, the decay curves at 828 nm were measured under the condition of p_{Xe} = 9.9 Torr and low pressures of Rg (p_{Ar} < 5.0 Torr or p_{Ne} < 6.2 Torr). Indeed, these curves fit a single exponential decay well. Then, the total decay rate constants for Ar and Ne can be deduced from a Stern–Volmer plot. These plots are shown in Figure 4. The total decay rate constants for Ar and Ne are listed in Table 1.

To deduce the value for $k_{1,2}^{Rg}$ (Rg = Ar or Ne), the curves at 828 nm were measured and fitted by a double exponential decay function under the condition of p_{Xe} = 4.0 Torr and relatively high pressure of Rg (Rg = Ar or Ne). These fits are marked by the green curves in Figure 2. Clearly, these two curves fit a double exponential function well. Then, a series of $\lambda_{+,-}$ can be obtained under the conditions of different p_{Rg}. The $\lambda_{+,-}$ can be illustrated by eq 13:

$$\lambda_{+,-} = \frac{A_{11} + A_{22} \pm \sqrt{(A_{11} - A_{22})^2 + 4A_{12}A_{21}}}{2} \tag{13}$$

where $A_{11} = k_{1,T}^{Rg}[Rg] + C_1$, $C_1 = k_{1,T}^{Xe}[Xe] + k_{1,r}$, $A_{22} = k_{2,T}^{Rg}[Rg] + C_2$, and $C_2 = k_{2,T}^{Xe}[Xe] + k_{2,r}$. Since $k_{1,2}^{Xe}[Xe]$ and $k_{2,1}^{Xe}[Xe]$ are low enough to be omitted, we can obtain $A_{12} = k_{1,2}^{Rg}[Rg]$, $A_{21} =$

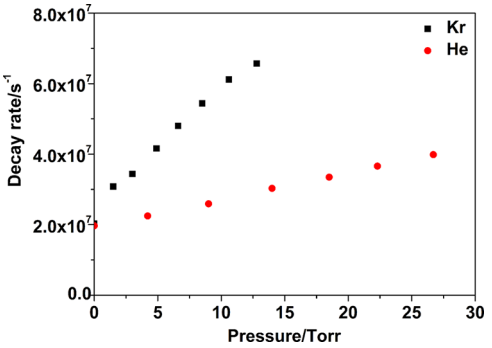

Figure 3. Stern–Volmer plots for the $6p[1/2]_0$ state in Kr and He buffer gases. The Xe pressure is 4.0 Torr. The energy of the excitation laser is 2.80 mJ. The $6p[1/2]_0$ atoms are directly prepared by the laser.

Table 1. Kinetic Parameters Measured by Stern–Volmer Plots[a]

kinetic parameters	this work	data from references
$k^{Kr}_{6p[1/2]_0,T}$	10.37 ± 0.53	11.0 ± 0.5 (ref 12)
$k^{Ar}_{6p[1/2]_0,T}$	15.29 ± 0.52	18.3 ± 0.6 (ref 15), 14.0 ± 1 (ref 12)
$k^{Ar}_{6p[1/2]_0,5d[1/2]_1}$	13.94 ± 0.30	17.0 ± 0.3 (ref 15), 10.0 (ref 12)
$k^{Ar}_{5d[1/2]_1,6p[1/2]_0}$	2.46 ± 0.05	3.0 ± 0.1 (ref 15), 1.8 (ref 12)
$k^{Ar}_{5d[1/2]_1,T}$	2.98 ± 0.60	3.4 ± 0.2 (ref 15), 3.8 (ref 12)
$k^{Ne}_{6p[1/2]_0,T}$	3.37 ± 0.11	3.4 ± 0.2 (ref 10)
$k^{Ne}_{6p[1/2]_0,5d[1/2]_1}$	3.24 ± 0.10	3.4 (ref 10)
$k^{Ne}_{5d[1/2]_1,6p[1/2]_0}$	0.57 ± 0.07	0.6 (ref 10)
$k^{Ne}_{5d[1/2]_1,T}$	0.68 ± 0.14	0.8 (ref 10)
$k^{He}_{6p[1/2]_0,T}$	2.29 ± 0.03	2.0 ± 0.2 (ref 10)

[a]All the units for the data shown in this table are in 10^{-11} cm^3 s^{-1}. For concise illustration, the unit is omitted.

DOI: 10.1021/acs.jpca.8b03238
J. Phys. Chem. A 2018, 122, 5361–5369

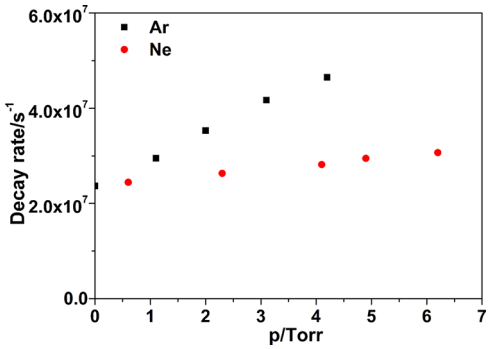

Figure 4. Stern–Volmer plots for the $6p[1/2]_0$ state in Ar and Ne buffer gases. The Xe pressure is 9.9 Torr. The energy of the excitation laser is 2.80 mJ. The $6p[1/2]_0$ atoms are directly prepared by laser.

$k_{2,1}^{Rg}[Rg] = 0.1766k_{1,2}^{Rg}[Rg]$. Then, eq 13 can be rewritten as eq 14:

$$\lambda_{+,-} = \frac{(k_{1,T}^{Rg} + k_{2,T}^{Rg})[Rg] + C_1 + C_2}{2} \pm \frac{\sqrt{((k_{1,T}^{Rg} - k_{2,T}^{Rg})[Rg] + (C_1 - C_2))^2 + 0.706 \times (k_{1,2}^{Rg}[Rg])^2}}{2} \quad (14)$$

Under the conditions of p_{Xe} = 4.0 Torr and p_{Rg} being relatively high, $C_1 - C_2$ can be omitted. Then, eq 14 can be rewritten as eq 15.

$$\lambda_{+,-} = \frac{(k_{1,T}^{Rg} + k_{2,T}^{Rg})[Rg] + C_1 + C_2}{2} \pm \frac{[Rg] \times \sqrt{(k_{1,T}^{Rg} - k_{2,T}^{Rg})^2 + 0.706 \times (k_{1,2}^{Rg})^2}}{2} \quad (15)$$

Then, $\frac{d\lambda_{+,-}}{d[Rg]}$ can be expressed as eq 16.

$$\frac{d\lambda_{+,-}}{d[Rg]} = \frac{(k_{1,T}^{Rg} + k_{2,T}^{Rg}) \pm \sqrt{(k_{1,T}^{Rg} - k_{2,T}^{Rg})^2 + 0.706 \times (k_{1,2}^{Rg})^2}}{2} \quad (16)$$

According to eq 16, the relationship between $\lambda_{+,-}$ and p_{Rg} is linear. Indeed, the relationship between $\lambda_{+,-}$ and p_{Rg} is linear as shown in Figure 5. This observation is consistent with previous studies.[12,15] Then, the values for $\frac{d\lambda_{+,-}}{d[Rg]}$ can be obtained by calculating the slope from these data. In eq 16, $k_{1,t}^{Rg}$ is known. The only unknown parameters that remain are $k_{2,t}^{Rg}$ and $k_{1,2}^{Rg}$. These can be deduced using the eq 16 and are listed in Table 1. Parameters reported in previous studies are also listed for comparison.

As shown in Table 1, the relaxation rate constants for $6p[1/2]_0 \rightarrow 5d[1/2]_1$ in Ar and Ne are 13.94×10^{-11} and 3.24×10^{-11} cm^3 s^{-1}, respectively. Accordingly, the ASE channel switching capability for Ar is significantly stronger than that for Ne as shown in Figure 1. The intensities for the ASE at 3408 nm ($6p[1/2]_0$–$6s'[1/2]_1$) and 3680 nm ($5d[1/2]_1$–$6p[1/2]_1$) are both strong under the condition of p_{Ne} = 205.3 Torr. However, under the condition of p_{Ar} = 136.0 Torr, the intensity of the ASE at 3408 nm ($6p[1/2]_0$–$6s'[1/2]_1$) is hardly visible, while the ASE at 3680 nm ($5d[1/2]_1$–$6p[1/2]_1$) is very strong.

In a brief, if the value of $k_{6p[1/2]_0,5d[1/2]_1}$ is high, A_{12} is accordingly high. Then, a substantial number of $5d[1/2]_1$ atoms can be populated. In addition, the value of $k_{5d[1/2]_1,6p[1/2]_0}$ is also high. Therefore, A_{21} in eq 7 cannot be omitted. Consequently, the energy-transfer processes between the $6p[1/2]_0$ and $5d[1/2]_1$ state are very rapid. Under this circumstance, these two states are coupled with each other. As a result, the decay curve at 828 nm fits a double exponential function. This is the reason why a high rate constant for the transfer of $6p[1/2]_0 \rightarrow 5d[1/2]_1$ can result in a double exponential decay for the $6p[1/2]_0$ state. As a result, the double exponential decay of the $6p[1/2]_0$ state normally coincides with an ASE channel switch. However, the situation for Kr is an exception. All the calculation results above satisfy the condition that the transfers between the $5d[1/2]_1$ state and the $6p[1/2]_0$ state are accomplished by two-state coupling, as described by eq 17. The mechanism for the transfer of $6p[1/2]_0 \rightarrow 5d[1/2]_1$ in Kr cannot involve two-state coupling. The energy difference between the $6p[1/2]_0$ state and the $5s[3/2]_2$ (Kr) state is only ~147 cm^{-1}. The $6p[1/2]_0$ atoms strongly tend to reach the $5s[3/2]_2$ (Kr) state.[12] The energy difference between the $5s[3/2]_2$ (Kr) state and the $5d[1/2]_1$ state is only ~12 cm^{-1}. The $5s[3/2]_2$ (Kr) atoms must have a high probability to reach the $5d[1/2]_1$ state. Consequently, the transfer processes of $6p[1/2]_0 \rightarrow 5d[1/2]_1$ in Kr are accomplished by two steps of near-resonance collision, as described by eq 18 and 19.

$$Xe(6p[1/2]_0) + Rg \xleftrightarrow{collision} Xe(5d[1/2]_1) + Rg \quad (17)$$

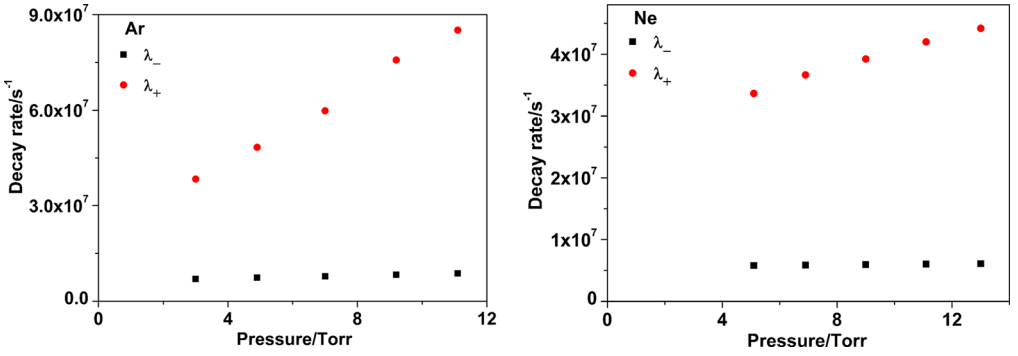

Figure 5. Stern–Volmer plots for the $\lambda_{+,-}$ in Ar and Ne buffer gases. The Xe pressure is 4.0 Torr. The energy of the excitation laser is 2.80 mJ. The $6p[1/2]_0$ atoms are directly prepared by laser.

DOI: 10.1021/acs.jpca.8b03238
J. Phys. Chem. A 2018, 122, 5361–5369

$$Xe(6p[1/2]_0) + Kr(s_0) \xrightarrow{\text{collision}} Xe(s_0) + Kr(5s[3/2]_2) \quad (18)$$

$$Kr(5s[3/2]_2) + Xe(s_0) \xrightarrow{\text{collision}} Xe(5d[1/2]_1) + Kr(s_0) \quad (19)$$

Although the relaxation rate constant for He for the transfer of $6p[1/2]_0 \rightarrow 5d[1/2]_1$ is very low, the relaxation rate for this transfer can be high under the condition of high He pressure. However, there is no ASE at 3680 nm ($5d[1/2]_1$–$6p[1/2]_1$), as shown in Figure 1, even under the condition of p_{He} = 305.7 Torr. Not only the transfer of $6p[1/2]_0 \rightarrow 5d[1/2]_1$ but also that of $6p[1/2]_0 \rightarrow 6p[i]_j$ can be reinforced. Then, the $6p[1/2]_0$ atoms tend to decay through the relaxation channel instead of the ASE channel. Moreover, relaxation rate for the $5d[1/2]_1$ state is also high under the condition of high He pressure. Therefore, the population inversion between the $5d[1/2]_1$ and $6p[1/2]_1$ is hard to form under the conditions of high He pressure. However, the situation may be different under the condition of high Xe pressure, since, under such a condition, the population of the $6p[1/2]_0$ state may also dramatically increase. Although the probability of relaxation increases, more $6p[1/2]_0$ atoms can produce $5d[1/2]_1$ atoms. The ASE at 3680 nm ($5d[1/2]_1$–$6p[1/2]_1$) probably emerges under this condition. Thus, ASE in the forward direction along the laser axis was observed under the condition of p_{Xe} = 216.0 Torr and E = 3.86 mJ. This result is shown in Figure 6. Clearly, there is

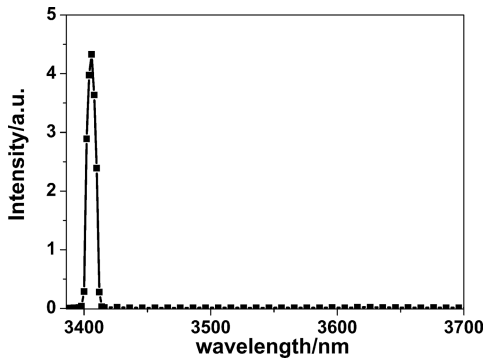

Figure 6. ASE spectra measured for Xe in the forward direction along the laser axis under the condition of p_{Xe} = 216.0 Torr and E = 3.86 mJ. The laser prepared state is the $6p[1/2]_0$ state.

no ASE at 3680 nm ($5d[1/2]_1$–$6p[1/2]_1$). The higher pressure may not only accelerate the transfer of $6p[1/2]_0 \rightarrow 5d[1/2]_1$ but also accelerate the process described in eq 3. The relaxation rate constant in eq 3 is as high as ~4.99×10^{-11} cm^3 s^{-1}.[21] Then, substantial $6p[1/2]_1$ atoms can be rapidly produced as indicated by eq 2 and 3. Consequently, the population inversion between the $5d[1/2]_1$ state and the $6p[1/2]_1$ state in high Xe pressure is also difficult to form.

In this work, the two ASE channels at 3408 nm ($6p[1/2]_0$–$6s'[1/2]_1$) and 3680 nm ($5d[1/2]_1$–$6p[1/2]_1$) compete with each other. Because of the small energy difference (~84 cm^{-1}) between the $6s'[1/2]_1$ state and the $6p[1/2]_1$ state, the energy transfer processes between these two states must be very rapid. Consequently, a series of processes related to one ASE channel can produce substantial atoms in the lower state of the other ASE channel. This can reduce the degree of population inversion. Under the condition of pure Xe, some $6p[1/2]_0$ atoms can arrive at the $5d[1/2]_1$ state by collision. However, a substantial number of $6p[1/2]_1$ atoms can be rapidly produced through eq 2 and 3 to destruct the population inversion between the $5d[1/2]_1$ and $6p[1/2]_1$ states. As a result, only the ASE at 3408 nm ($6p[1/2]_0$–$6s'[1/2]_1$) can be generated. When the Kr, Ar or Ne atoms are filled into the system, the transfer of $6p[1/2]_0 \rightarrow 5d[1/2]_1$ can be significantly accelerated to produce population inversion between the $5d[1/2]_1$ and $6p[1/2]_1$ state. Then, the ASE at 3680 nm ($5d[1/2]_1$–$6p[1/2]_1$) is rapidly generated to populate a substantial number of $6p[1/2]_1$ atoms. Accordingly, many $6s'[1/2]_1$ atoms can also be produced. This reduces the degree of population inversion between the $6p[1/2]_0$ and $6s'[1/2]_1$ states. Thus, the ASE at 3408 nm ($6p[1/2]_0$–$6s'[1/2]_1$) is inhibited. To some extent, the ASE channel switch effect shown in Figure 1 is attributed to this reason.

The buffer gases can significantly increase the probability of relaxation. They may accelerate not only the transfer of $6p[1/2]_0 \rightarrow 5d[1/2]_1$ but also some transfers of $6p[1/2]_0 \rightarrow 6p[i]_j$. To study this subject systematically, the time-resolved fluorescence curves were measured to characterize the populations of the five secondary $6p[i]_j$ states in the buffer gases including Kr, Ar, Ne, and He. The results are shown in Figure 7. When a He buffer gas is used, the intensity at 823 nm significantly increases. This indicates that the He atoms can accelerate the transfer of $6p[1/2]_0 \rightarrow 6p[3/2]_2$. Although the total decay rate constant for the $6p[1/2]_0$ state in He is only (2.29 ± 0.03) $\times 10^{-11}$ cm^3 s^{-1}, the collisional rate constant for the transfer of $6p[1/2]_0 \rightarrow 6p[3/2]_2$ probably take a great proportion. The intensity at 882 nm slightly increases. Although the rate constant for the transfer of $6p[1/2]_0 \rightarrow 6p[5/2]_3$ may not be very high, the rate of this transfer can be higher for high He pressures. The intensities at 916 and 904 nm hardly change. Thus, the probabilities of the transfers of $6p[1/2]_0 \rightarrow 6p[3/2]_1$, $6p[5/2]_2$ are very small in He. The intensities at 980 nm in He gradually decrease for increasing pressure. He atoms cannot selectively accelerate the transfer of $6p[1/2]_0 \rightarrow 5d[1/2]_1$. Moreover, more He atoms can drive more $6p[1/2]_0$ atoms to decay through the relaxation channels instead of ASE at 3408 nm ($6p[1/2]_0$–$6s'[1/2]_1$). Therefore, fewer $6p[1/2]_1$ atoms can be produced. When a Ne buffer gas is used, the intensities at 823 nm, 916 nm, 904 nm hardly change. Only the intensity at 882 nm slightly increases. According to Table 1, $k^{Ne}_{6p[1/2]_0,5d[1/2]_1}$ takes a great proportion of $k^{Ne}_{6p[1/2]_0,T}$, then the tendencies for the transfers of $6p[1/2]_0 \rightarrow 6p[3/2]_2$, $6p[3/2]_1$, $6p[5/2]_2$ are very small in Ne. The peak height at 980 nm does not change much in Ne. However, the rising edge becomes steeper following the addition of Ne atoms into the cell. This indicates that the $6p[1/2]_1$ atoms are produced much more rapidly. The transfer processes for $6p[1/2]_0 \rightarrow 6p[1/2]_1$ through ASE at 3408 nm include an endothermic process ($6s'[1/2]_1 \rightarrow 6p[1/2]_1$), while those transfer processes occurring through ASE at 3680 nm involve an exothermic process ($6p[1/2]_0 \rightarrow 5d[1/2]_1$). Usually, the exothermic process is easier to generate. For an Ar buffer gas, the intensities at 823 nm, 916 nm, 904 nm hardly change, similar to those found in Ne. Only the intensity at 882 nm slightly increases. However, the intensities at 980 nm increase dramatically. This results from the high rate constant of Ar for the transfer of $6p[1/2]_0 \rightarrow 5d[1/2]_1$. A series of processes related to the ASE at 3680 nm ($5d[1/2]_1$–$6p[1/2]_1$) can drive more $6p[1/2]_0$ atoms to reach the $6p[1/2]_1$ state. When a Kr buffer gas is used, the change in the fluorescence curves at 980

DOI: 10.1021/acs.jpca.8b03238
J. Phys. Chem. A 2018, 122, 5361–5369

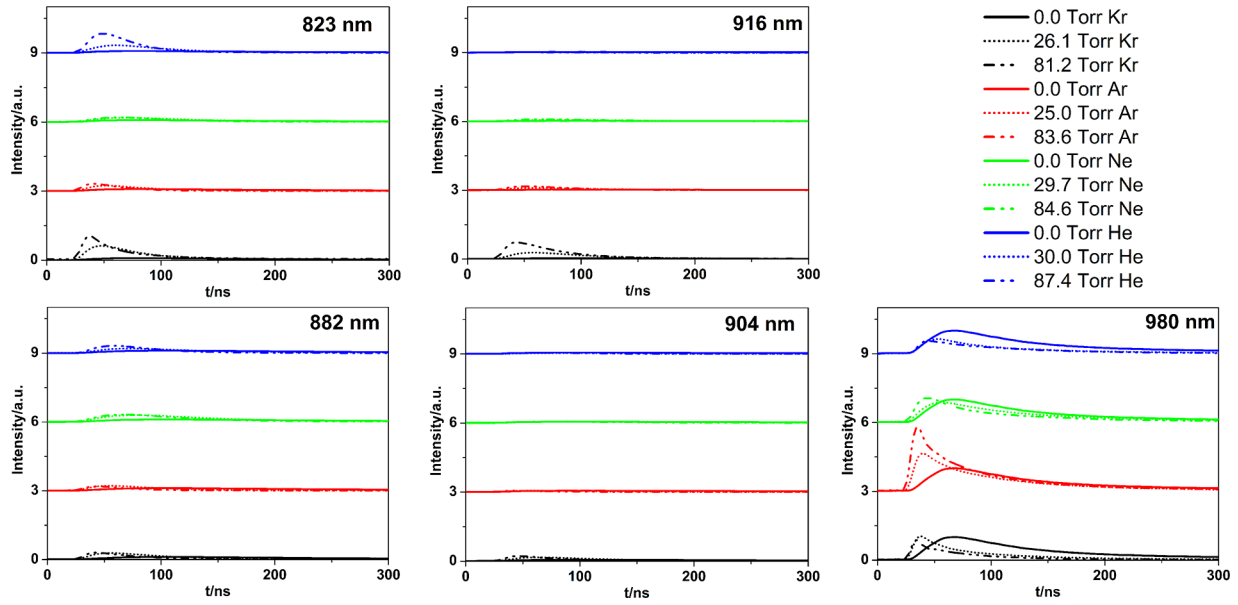

Figure 7. Time-resolved fluorescence curves measured at 823 nm ($6p[3/2]_2$–$6s[3/2]_2$), 916 nm ($6p[3/2]_1$–$6s[3/2]_1$), 882 nm ($6p[5/2]_3$–$6s[3/2]_2$), 904 nm ($6p[5/2]_2$–$6s[3/2]_2$), and 980 nm ($6p[1/2]_1$–$6s[3/2]_2$) for varying buffer gases. The $6p[1/2]_0$ state is directly prepared by the laser. The Xe pressure is 6.0 Torr. The energy of the excitation laser is 2.80 mJ. For clear comparison, the intensity of the different gases is moved upward 3 au stepwise.

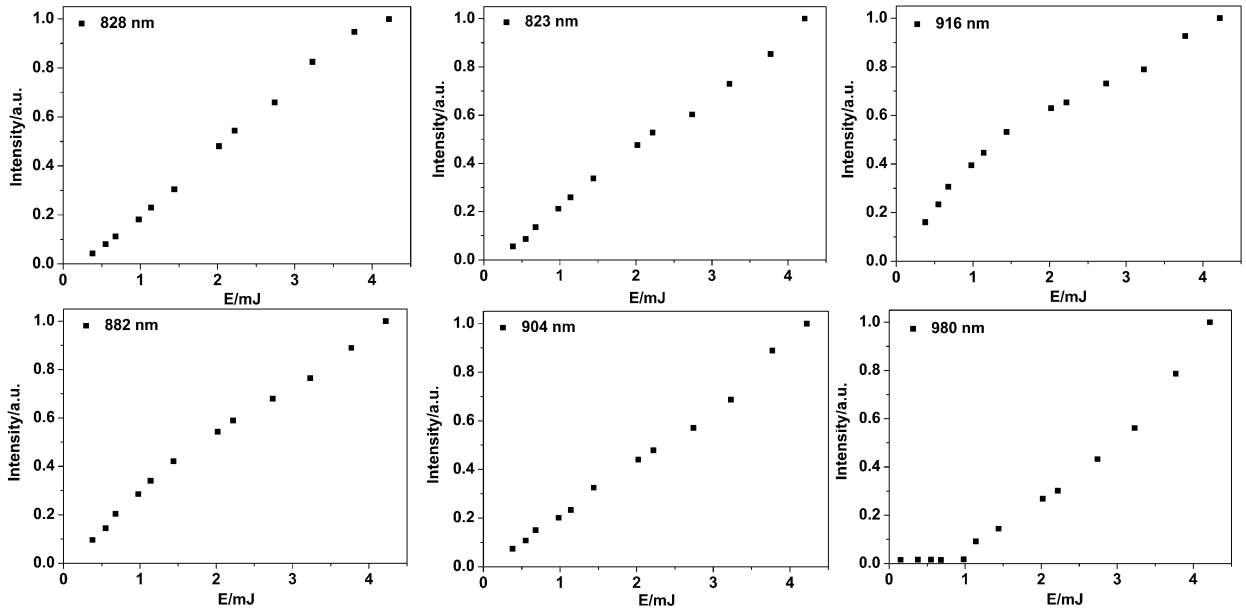

Figure 8. Normalized fluorescence intensities under the conditions of different excitation laser energies. The Xe and Kr pressures are 7.8 and 61.1 Torr, respectively.

nm in Kr acts like that in Ne. Although the ASE channel switch effect in Kr is as strong as that in Ar (shown in Figure 1), the intensities at 980 nm in Kr are much lower than that in Ar. In comparison with the transfer of $6p[1/2]_0 \rightarrow 5d[1/2]_1$ in Ar, the transfer of $6p[1/2]_0 \rightarrow 5d[1/2]_1$ in Kr needs to pass through the $5s[3/2]_2$ (Kr) state. This increases the probability for quenching. As a result, fewer $6p[1/2]_1$ atoms are produced in Kr compared with that in Ar. The intensities at 882 nm in these four gases all slightly increase. The radiative branching ratio at 882 nm is 100%. Then, this fluorescence line should be easier to observe compared with other lines. The unexpected phenomenon is that the intensities at 823 and 916 nm are significantly increased in Kr. In addition, the intensity at 904 nm is also slightly increased. This is much different from the changes in intensity found in Ar, Ne, and He. This indicates that the probabilities for $6p[1/2]_0 \rightarrow 6p[3/2]_2$, $6p[3/2]_1$ in Kr dramatically increase. Moreover, the probability for $6p[1/2]_0 \rightarrow 6p[5/2]_2$ in Kr also increases.

The following two mechanisms are proposed to illustrate the microscopic processes. The first one is the ASE mechanism. Similar to the mechanism of $6p[1/2]_0 \rightarrow 6p[1/2]_1$, the Kr atoms may accelerate a transfer from the $6p[1/2]_0$ state to one $5d[i]_j$ state near the $6p[1/2]_0$ state. Then, the ASE of $5d[i]_j$–$6p[3/2]_2$, $6p[3/2]_1$, $6p[5/2]_2$ are rapidly generated. Consequently, a substantial number of $6p[3/2]_2$, $6p[3/2]_1$, and $6p[5/2]_2$ atoms are produced. The second mechanism involves

DOI: 10.1021/acs.jpca.8b03238
J. Phys. Chem. A 2018, 122, 5361−5369

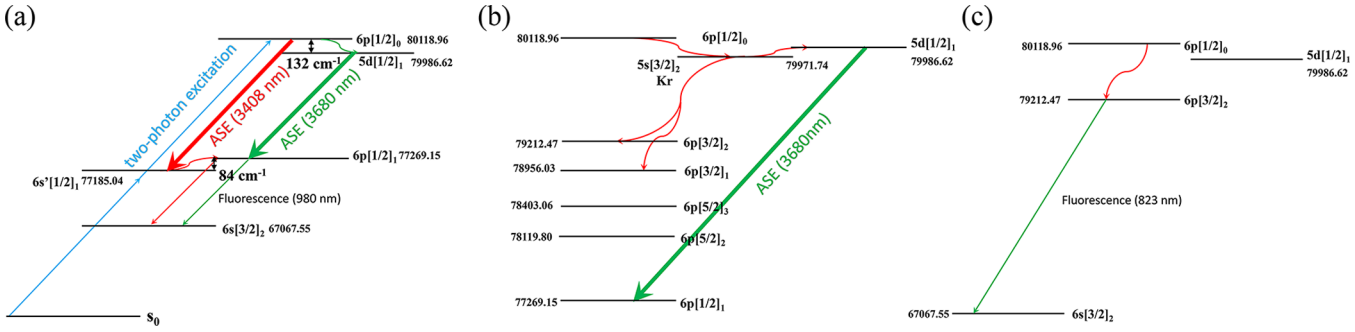

Figure 9. Primary energy-transfer processes for Xe ($6p[1/2]_0$) atoms in Ar (a), Ne (a), Kr (b), and He (c).

collisional relaxation through the $5s[3/2]_2$ state of Kr as the intermediate state. When the $6p[1/2]_0$ atoms collide with Kr, they show a strong tendency to generate $5s[3/2]_2$ (Kr) atoms eq 18. Then, the $6p[3/2]_2$, $6p[3/2]_1$, and $6p[5/2]_2$ atoms can be produced by relaxation of the $5s[3/2]_2$ (Kr) atoms. The energy-transfer processes from $5s[3/2]_2$ (Kr) to Xe mainly give rise to the $6p[3/2]_2$ and $6p[3/2]_1$ states.[17]

If the ASE is the primary mechanism, the $5d[i]_j$ state probably refers to the $5d[3/2]_2$ state (80322.75 cm^{-1}). Only the emission wavelength for $5d[3/2]_2$–$6p[5/2]_2$ can be observed by our detector. However, no ASE signals were measured at 4539 nm ($5d[3/2]_2$–$6p[5/2]_2$). To further identify a reasonable mechanism, the intensities of the spontaneous emissions were measured under the conditions of different excitation laser energies. The results are shown in Figure 8. If $6p[i]_j$ atoms are produced by the mechanism of ASE, spontaneous emission involving this upper state should have a threshold. Obviously, the spontaneous emission at 980 nm has a threshold at ~1.0 mJ, because the $6p[1/2]_1$ atoms are produced by a series process related to ASE at 3680 nm. However, the spontaneous emission at 823, 916, and 904 nm does not have an obvious threshold. Therefore, the mechanism based on ASE is denied. A reasonable primary mechanism is collisional relaxation. This can be described using eqs 18 and 20.

$$\mathrm{Kr}(5s[3/2]_2) + \mathrm{Xe}(s_0) \xrightarrow{\text{collision}} \mathrm{Xe}(6p[3/2]_2, 6p[3/2]_1, 6p[5/2]_2) + \mathrm{Kr}(s_0) \quad (20)$$

In summary, Ar and Ne atoms can accelerate the transfer of $6p[1/2]_0 \rightarrow 5d[1/2]_1$. Thus, Ar and Ne atoms can switch the ASE channel from 3408 nm ($6p[1/2]_0$–$6s'[1/2]_1$) to 3680 nm ($5d[1/2]_1$–$6p[1/2]_1$). The transfer of $6p[1/2]_0 \rightarrow 5d[1/2]_1$ in Ar and Ne is accomplished by two-state coupling. The high rate constant for the transfer of $6p[1/2]_0 \rightarrow 5d[1/2]_1$ can result in a high rate constant for the transfer of $5d[1/2]_1 \rightarrow 6p[1/2]_0$. Consequently, the ASE channel switch effect always coincides with a double exponential decay for the spontaneous emission at 828 nm ($6p[1/2]_0$–$6s[3/2]_1$) in Ar and Ne. On the basis of the rate equations for two-state coupling, the value for $k^{\mathrm{Rg}}_{6p[1/2]_0,5d[1/2]_1}$ (Rg = Ar or Ne) was deduced. We found that the value of $k^{\mathrm{Ar}}_{6p[1/2]_0,5d[1/2]_1}$ is higher than that of $k^{\mathrm{Ne}}_{6p[1/2]_0,5d[1/2]_1}$. Therefore, the ASE channel switch effect for Ar is stronger than that for Ne. The primary processes in Ar and Ne are illustrated in Figure 9a.

The energy-transfer kinetic processes for $6p[1/2]_0$ atoms in Kr are much more complicated than those in Ar and Ne. The Kr atoms also show an ASE channel switch effect. Such atoms can also accelerate the transfer of $6p[1/2]_0 \rightarrow 5d[1/2]_1$. Unlike that found in Ar and Ne, the kinetic processes for the transfer of $6p[1/2]_0 \rightarrow 5d[1/2]_1$ in Kr involve two steps of near-resonance collision through the $5s[3/2]_2$ (Kr) state as the intermediate state. Although the ASE channel switch effect for Kr is as strong as that for Ar, the tendency for $6p[1/2]_0$ atoms to reach the $6p[1/2]_1$ state in Kr is much weaker than that in Ar. The complicated processes in Kr lead to a higher probability for relaxation to other states. Indeed, we found that the transfers of $6p[1/2]_0 \rightarrow 5s[3/2]_2$ (Kr) $\rightarrow 6p[3/2]_2$, $6p[3/2]_1$ are also considerably strong. These channels compete with the transfer of $6p[1/2]_0 \rightarrow 5s[3/2]_2$ (Kr) $\rightarrow 5d[1/2]_1$. Therefore, fewer $6p[1/2]_0$ atoms can reach the $6p[1/2]_1$ state. The primary kinetic processes in Kr are illustrated in Figure 9b.

He atoms cannot accelerate the transfer of $6p[1/2]_0 \rightarrow 5d[1/2]_1$. Thus, He atoms cannot switch the ASE channels. In addition, we found that the probability for the transfer of $6p[1/2]_0 \rightarrow 6p[3/2]_2$ in He significantly augments. The primary kinetic processes in He are illustrated in Figure 9c.

IV. CONCLUSION

The energy-transfer processes for $6p[1/2]_0$ atoms in Kr, Ar, Ne, and He buffer gases were studied. The primary process in Ar or Ne buffer gas is accelerating transfer of $6p[1/2]_0 \rightarrow 5d[1/2]_1$ by two-state coupling. We found that the value of $k^{\mathrm{Ar}}_{6p[1/2]_0,5d[1/2]_1}$ is higher than that of $k^{\mathrm{Ne}}_{6p[1/2]_0,5d[1/2]_1}$. The primary processes in Kr buffer gas are accelerating transfers of $6p[1/2]_0 \rightarrow 5s[3/2]_2$ (Kr) $\rightarrow 5d[1/2]_1$, $6p[3/2]_2$, $6p[3/2]_1$. The primary process in He buffer gas is accelerating transfer of $6p[1/2]_0 \rightarrow 6p[3/2]_2$.

The $5s[3/2]_2$ (Kr) state plays an important role in the energy-transfer kinetics for $6p[1/2]_0$ atoms. Kr is probably an ideal buffer gas for the Xe laser system. Further work will enable one to select proper states and the most suitable buffer gas for obtaining a DPRGL based on Xe.

AUTHOR INFORMATION

Corresponding Author

*(J.G.) E-mail: jingweiguo@dicp.ac.cn.

ORCID

Jingwei Guo: 0000-0001-9158-7828

Notes

The authors declare no competing financial interest.

ACKNOWLEDGMENTS

This work is supported by the National Natural Science Foundation of China (Grant Nos. 11475177, 61505210) and Key Laboratory of Chemical Laser Foundation (KLCL 2017).

DOI: 10.1021/acs.jpca.8b03238
J. Phys. Chem. A 2018, 122, 5361−5369

REFERENCES

(1) Kabir, M. H.; Heaven, M. C. Energy Transfer Kinetics of the $np^5(n+1)p$ Excited States of Ne and Kr. *J. Phys. Chem. A* **2011**, *115*, 9724−9730.

(2) Han, J.; Heaven, M. C. Gain and Lasing of Optically Pumped Metastable Rare Gas Atoms. *Opt. Lett.* **2012**, *37*, 2157−2159.

(3) Han, J.; Glebov, L.; Venus, G.; Heaven, M. C. Demonstration of a Diode-pumped Metastable Ar Laser. *Opt. Lett.* **2013**, *38*, 5458−5461.

(4) Han, J.; Heaven, M. C. Kinetics of Optically Pumped Ar Metastables. *Opt. Lett.* **2014**, *39*, 6541−6544.

(5) Rawlins, W. T.; Galbally-Kinney, K. L.; Davis, S. J.; Hoskinson, A. R.; Hopwood, J. A.; Heaven, M. C. Optically Pumped Microplasma Rare Gas Laser. *Opt. Express* **2015**, *23*, 4804−4813.

(6) Han, J.; Heaven, M. C.; Moran, P. J.; Pitz, G. A.; Guild, E. M.; Sanderson, C. R.; Hokr, B. Demonstration of a CW Diode-pumped Ar Metastable Laser Operating at 4 W. *Opt. Lett.* **2017**, *42*, 4627−4630.

(7) Yang, Z.; Yu, G.; Wang, H.; Lu, Q.; Xu, X. Modeling of Diode Pumped Metastable Rare Gas Lasers. *Opt. Express* **2015**, *23*, 13823−13832.

(8) Mikheyev, P. A. Optically Pumped Rare-gas Lasers. *Quantum Electron.* **2015**, *45*, 704−708.

(9) Ku, J. K.; Setser, D. W. Collisional Deactivation of Xe ($5p^56p$) States in Xe and Ar. *J. Chem. Phys.* **1986**, *84*, 4304−4316.

(10) Xu, J.; Setser, D. W. Collisional Deactivation Studies of the Xe (6p) States in He and Ne. *J. Chem. Phys.* **1991**, *94*, 4243−4251.

(11) Inoue, G.; Ku, J. K.; Setser, D. W. Laser Induced Fluorescence Study of Xe ($5p^56p$, $5p^56p'$, $5p^57p$, and $5p^56d$) States in Ne and Ar: Radiative Lifetimes and Collisional Deactivation Rate Constants. *J. Chem. Phys.* **1984**, *81*, 5760−5774.

(12) Xu, J.; Setser, D. W. Deactivation Rate Constants and Product Branching in Collisions of the Xe (6p) States with Kr and Ar. *J. Chem. Phys.* **1990**, *92*, 4191−4202.

(13) Böwering, N.; Bruce, M. R.; Keto, J. W. Collisional Deactivation of Two-photon Laser Excited Xenon $5p^56p$. I. State-to-state Reaction Rates. *J. Chem. Phys.* **1986**, *84*, 709−714.

(14) Böwering, N.; Bruce, M. R.; Keto, J. W. Collisional Deactivation of Two-photon Laser Excited Xenon $5p^56p$. II. Lifetimes and Total Quench Rates. *J. Chem. Phys.* **1986**, *84*, 715−726.

(15) Bruce, M. R.; Layne, W. B.; Whitehead, C. A.; Keto, J. W. Radiative Lifetimes and Collisional Deactivation of Two-photon Excited Xenon in Argon and Xenon. *J. Chem. Phys.* **1990**, *92*, 2917−2926.

(16) Alford, W. J. State-to-state Rate Constants for Quenching of Xenon 6p Levels by Rare Gases. *J. Chem. Phys.* **1992**, *96*, 4330−4340.

(17) Sobczynski, R.; Setser, D. W. Improvements in the Generation and Detection of $Kr(^3p_0)$ and $Kr(^3p_2)$ Atoms in a Flow Reactor: Decay Constants in He Buffer and Total Quenching Rate Constants for Xe, N_2, CO, H_2, CF_4, and CH_4. *J. Chem. Phys.* **1991**, *95*, 3310−3324.

(18) Eichhorn, C.; Fritzsche, S.; Lohle, S.; Knapp, A.; Auweter-Kurtz, M. A. Time-Resolved Fluorescence Spectroscopy of Two-Photon Laser-Excited 8p, 9p, 5f, and 6f Levels in Neutral Xenon. *Phys. Rev. E* **2009**, *80*, 026401.

(19) He, S.; Guan, Y.; Liu, D.; Xia, X.; Gai, B.; Hu, S.; Guo, J.; Sang, F.; Jin, Y. Energy Transfer Kinetics Driven by Midinfrared Amplified Spontaneous Emission after Two-Photon Excitation from Xe (s_0) to the Xe ($6p[1/2]_0$) State. *J. Phys. Chem. A* **2017**, *121*, 3430−3436.

(20) Tam, A.; Moe, G.; Happer, W. Particle Formation by Resonant Laser Light in Alkali-metal Vapor. *Phys. Rev. Lett.* **1975**, *35*, 1630−1633.

(21) Sadeghi, N.; Sabbagh, J. Collisional Transfer between the $6s'[1/2]_{0,1}$ and $6p[1/2]_1$ Xenon Levels. *Phys. Rev. A: At., Mol., Opt. Phys.* **1977**, *16*, 2336−2345.

DOI: 10.1021/acs.jpca.8b03238
J. Phys. Chem. A 2018, 122, 5361−5369